XIV International Conference on Computational Plasticity. Fundamentals and Applications
COMPLAS 2017
E. Oñate, D.R.J. Owen, D. Peric and M. Chiumenti (Eds)

3D-MESOMECHANICAL ANALYSIS OF EXTERNAL SULFATE ATTACK IN CONCRETE

A. PÉREZ*, C.RIERA*, C.M. LÓPEZ* AND I.CAROL*

* Department of Civil and Environmental Engineering
Universidad Politécnica de Cataluña
Jordi Girona 1, Edif. D2, E-08034 Barcelona, Spain
e-mail:adria.perez@upc.edu, carlos.maria.lopez@upc.edu, ignacio.carol@upc.edu

Key words: External sulfate attack, Concrete degradation, Finite element method, Interface element, Meso-mechanical analysis.

Abstract: The present study focuses on degradation of concrete by external sulfate attack. The numerical model developed by the MECMAT/UPC group, incorporates coupled C-M analysis using a meso-mechanical approach with discrete cracking, using the MEF and zero thickness interface elements with a constitutive law based on nonlinear fracture mechanics concepts. Examples of application are run on 2D and 3D samples, with geometries and FE meshes generated with a code developed also in-house. The numerical analysis is carried out using two independent codes and a "staggered" procedure. The first code performs the mechanical analysis and the second the diffusive/reaction chemical problem. 2D uncoupled and coupled analysis are presented and discussed. Preliminary coupled 3D results are also presented and compared with equivalent 2D results, and the differences are detected and analyzed.

1 INTRODUCTION

External sulfate attack is a chemical-mechanical degradation process that can lead to differential material expansions producing the type of cracking known as concrete "spalling" (figure 1), loss of strength and even the complete disintegration of the material under severe attack conditions. The main conditions that have to be fulfilled are the existence of a medium rich in sulfates, a high permeability (or diffusivity) of the concrete and the presence of a humid environment, which favors the general diffusion of sulfates [1]. Three processes are present in the attack:

1) Transport of sulfate ions through the pore network, mainly controlled by the permeability of the concrete (being the water/cement ratio the key parameter), as well as through the cracking system,

2) chemical reactions between the cement paste components and the sulfate ions (once these ions have entered the material, the type of cement and the content of aluminates will mainly determine the importance of reactions that may occur),

3) expansion phenomena as a consequence of the formation of new crystalline phases.

Figure 1: Cubic mortar specimen under the effects of the external magnesium sulfate attack at 360 days [2]

The presence of sulfates from external sources results in the formation of new phases inside the concrete such as secondary ettringite and gypsum. Most of the experimental evidence has shown that secondary ettringite formation is the major factor involved in expansions [3-5].

The intensity of the attack (or degree of degradation) depends on the quality of the concrete (cement type, w/c ratio, mineral additions or the concrete deterioration before the sulfate attack) and the environmental conditions (concentration, distribution and type of sulfates, humidity, temperature, pH of the solution, combined effect of different degradation processes, etc.). A complete treatment of the problem should involve both chemical and mechanical aspects of sulfate ingress, and its consequences on overall behavior, in order to reliably predict the durability of the concrete structures under sulfate attack.

In recent years, the research group of "Mechanics of Materials" at UPC has developed and consolidated a methodology for the numerical analysis of concrete and other heterogeneous quasi-brittle materials under mechanical and environmental actions, considering the corresponding THMC couplings. In the approach employed, a main focus is on cracking and fracture via a discrete approach using zero-thickness interface elements, which is combined with a meso-level representation of the main aggregate particles. Interface elements are pre-inserted along all lines in the FE mesh, which therefore become potential crack lines, equipped with a traction-separation constitutive model based on principles of non-linear fracture mechanics [6, 7].

This work focuses on the study of the external sulfate attack problem in concrete. First, results of a 2D analysis are presented, and then preliminary results of the extension of the 3D analysis are also presented. The study is an extension of a previous work [8, 9], in which the numerical formulation of the model was developed and some application examples in 2D were also presented. Subsequently, the study was continued in [10, 11] with an extension of the analysis with different size samples in 2D and 3D.

2 DESCRIPTION OF THE DIFUSSION/REACTION MODEL

The model is based in the formulation proposed by Mobasher [12] with the introduction of some improvements [8]. Due to the complexity of the problem, in [12] a simplified point of view of the problem has been considered, in which the external sulfate attack can be analyzed by the diffusion of a single type of ion, the sulfate ions.

It is assumed that the incoming sulfates react first with the portlandite to form gypsum ($C\overline{S}H_2$), and subsequently react with the different phases of non-diffusive calcium aluminates

in the hydrated cement paste, eventually forming secondary ettringite. A further reaction of ettringite formation, not considered in the original model [12], can also be added from the alumina-ferrite phase, resulting in a total of 4 possible reactions shown in expression (1).

$$\begin{aligned} &C_4AH_{13} + 3C\bar{S}H_2 + 14H \rightarrow C_6A\bar{S}_3H_{32} + CH \\ &C_4A\bar{S}H_{12} + 2C\bar{S}H_2 + 16H \rightarrow C_6A\bar{S}_3H_{32} \\ &C_3A + 3C\bar{S}H_2 + 26H \rightarrow C_6A\bar{S}_3H_{32} \\ &3C_4AF + 12C\bar{S}H_2 + xH \rightarrow 4\left(C_6A\bar{S}_3H_{32}\right) + 2\left[(A,F)H_3\right] \end{aligned} \tag{1}$$

While in [12] a grouped reaction is considered to simplify the analysis, in the formulation developed it is possible to treat each of the reactions separately, thus allowing consideration of different kinetics for each individual reaction [8].However, the kinetics of the individual reactions for the formation of ettringite are a priori unknowns, so that it may be convenient to proceed as in [8] where the first three reactions presented in (1) have been grouped, in a unique expression given by:

$$CA + q\bar{S} \rightarrow C_6A\bar{S}_3H_{32} \tag{2}$$

where q is the stoichiometric weighted coefficient of the grouped reaction. Reaction (2), takes place according to the availability of calcium sulfates and aluminates, which is determined in time and space through a second order diffusion-reaction equation for the concentration of sulfates (U [mol/m^3]) plus an equation for the decrease of calcium aluminate:

$$\frac{\partial U}{\partial t} = \frac{\partial}{\partial x}\left(D_U \frac{\partial U}{\partial x}\right) - kUC \tag{3}$$

$$\frac{\partial C}{\partial t} = -k\frac{UC}{q} \tag{4}$$

where C [mol/m^3] is the quantity of calcium aluminate equivalent by the grouping of the reactions (CA in equation (2)), and k is the grouped sulfate reaction rate.

The formulation presented in [12] considers an increase of the chemical diffusion coefficient when microcracking of the concrete occurs, using a damage variable. In the model developed in [8, 9] and used in this work, an improvement is included, considering that the diffusion coefficient decreases as the pores are filled with the precipitated chemicals. On the other hand, the diffusion through the cracks is explicitly considered with the use of the interface elements. In this way, the model used considers the decrease of the diffusivity due to the filling of the pores, simultaneously with an increase of the effective general diffusivity due to cracking phenomena [8, 9]. For this, a variation of the diffusion coefficient has been adopted in terms of a scale function according to the following expressions:

$$D_\Phi\left(\Phi_{cap}\right) = D_0 + \left(D_1 - D_0\right) f\left(\beta_D, \Phi_{cap}\right) \tag{5}$$

$$\text{with } f\left(\beta_D, \Phi_{cap}\right) = \frac{e^{-\beta_D}\xi}{1 + \left(e^{-\beta_D} - 1\right)\xi} \text{ and } \xi = \left(\Phi_{cap}/\Phi_{ini}\right) \tag{6}$$

$$\Phi_{ini} = v_c \cdot \left(\frac{w/c - 0.36\alpha}{w/c + 0.32}\right) \tag{7}$$

$$\Phi_{cap} = \Phi_{ini} - \alpha_s CA_{react} \text{ if } \alpha_s CA_{react} < \Phi_{ini} \text{ (else 0)} \tag{8}$$

where D_0, D_1, are lower and upper reference values, respectively, β_D is a parameter that determines the non linearity of the function, Φ_{ini} is the initial capillary porosity, Φ_{cap} is the updated capillary porosity that takes into account the increase of ettringite, ν_c is the volumetric fraction of cement, *w/c* is the ratio water-cement, α is the hydratation level and α_s y CA_{react} are defined later. Figure 2 shows the variation of the proposed law for β_D = 1.5, which is compared with other formulations of the literature (normalized values of diffusion coefficient and capillary porosity).

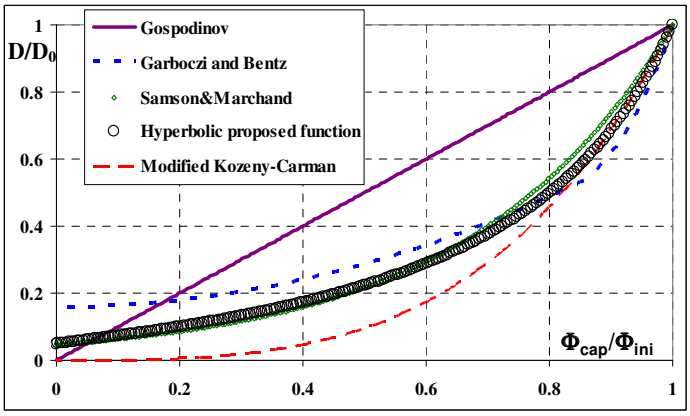

Figure 2: Comparison of the law of variation of the diffusion coefficient proposed in this work [8] with other formulations.

It is assumed that ettringite is the only product of the reactions that produce expansions. The volumetric strain is obtained from the amount of reacted calcium aluminate and the volume change associated therewith. For any of the individual reactions shown above, the volumetric change can be calculated as [12]:

$$\frac{\Delta V_i}{V_i} = \frac{m^{ettr}}{m^i + a_i \cdot m^{gypsum}} - 1 \tag{9}$$

where m^i is the molar volume [m^3/mol] of each chemical species and a_i is the stoichiometric coefficient involved in each reaction. To calculate the total volumetric strain, it is necessary to calculate the amount of reacted alumina phases (CA_{react} in the case of the grouped reaction and C^i_{react} for the extended model). For the complete version of the model, the volumetric deformation is calculated as:

$$\varepsilon_v(t) = \sum_{i=1}^{n} C^i_{react} \frac{\Delta V_i}{V_i} \overline{m}_i - f \cdot \Phi_{ini} \tag{10}$$

$$\overline{m}_i = m_i + a_i \cdot m^{gypsum} \quad \text{and} \quad C^i_{react} = C^i_0 - C^i_{unr} \tag{11}$$

where C_0^i represents the initial concentration of the different alumina phases, C_{unr}^i is the amount of non-reacted aluminates (given by the updated values of the internal values) and *f* is the porosity fraction of the capillary porosity that has to be filled before any expansion occurs.

For the simplified model, an average scheme for the different phases is used again, in which the increase of volume is related to the calcium aluminate reacted by a coefficient α_s. The typical values of *f* found by inverse analysis are in the range of 0.05-0.40 [12]. Additional details of the model and the verification tests can be found in [8, 9].

3 MESOMECHANICAL MODEL

3.1 Geometry and mesh generation

The numerical simulation is based on a meso-structural model in which the largest aggregate particles are represented explicitly, surrounded by a homogeneous matrix representing the average behavior of mortar plus the smaller aggregates. The shape and distribution of the large aggregate particles are randomly generated by a procedure based on the Voronoi-Delaunay theory [13]. In order to capture the main potential crack trajectories, zero-thickness interface elements are inserted a priori of the analysis, along all the aggregate-mortar and some of the mortar-mortar mesh lines.

3.2 Constitutive law for interface elements

The zero-thickness interface elements are equipped with a nonlinear constitutive law based on elasto-plasticity and concepts of fracture mechanics, which is formulated in terms of normal and shear components of the stress on the interface plane and the corresponding relative displacement variables. The initial loading (failure) surface $F = 0$ is given as three-parameter hyperbola (tensile strengthχ, asymptotic cohesion *c* and asymptotic friction angle tanϕ). The evolution of *F* (hardening-softening laws), is based on the internal variable W_{cr} (work spent in fracture processes), with the two material parameters G_F^I and G_F^{IIa} that represent the classical fracture energy in Mode I, plus a second fracture energy for an "asymptotic" Mode IIa under shear and high confinement. A more detailed description of this elasto-plastic constitutive law can be found in the literature [6, 7]. Results of the meso-mechanical model for normal concrete specimens subject to a variety of loading cases in 2D and 3D can also be found elsewhere [7, 8, 14, 15].

3.3 Chemo-Mechanical Coupling

The chemo-mechanical coupling (CM) has been achieved using a "staggered" approach that relates the two independent codes. For each time step, the first code performs the nonlinear diffusion-reaction analysis, and the results in terms of local expansions are imposed in the second code, solving the mechanical problem. The new displacement field obtained from the mechanical problem will modify the diffusion-reaction process due to the cracking, accelerating the sulfate ingress inside the specimen. As a result, this loop must be successively repeated within each time step until a certain tolerance is satisfied. The same FEM mesh is used for both analyses, using zero-thickness interface elements with double-nodes, whose formulation for the diffusion problem is explained in [16].

4 RESULTS

Results of 2D and 3D coupled calculations are presented in which the samples are immersed in a solution of 5% sodium sulfate, corresponding to a concentration of 35.2 mol/m^3. Both the 2D and 3D meshes have a 26% aggregate fraction of the total volume and the same parameters that characterize a CEM I52.5N/SR concrete have been adopted. The parameters of the chemical-reaction problem are: D_1=1.70x10^{-03}, k= 2x10^{-05}(m^3/(mol·day)), q=3, f=0.05, w/c=0.5, α=0.9, D_0/D_1=5x10^{-02}, β_D=1.5, α_s=1.33x10^{-04}, $[C_3A]_{inicial}$=200(mol/m^3). For the mechanical analysis, the aggregate and the mortar are considered linear elastic with parameters: E=70000 MPa (aggregates), E=25000 MPa (mortar) and υ=0.20 (both). For the aggregate-mortar interfaces the parameters are: K_N=K_T=100000 MPa/mm, $tan\phi_0$=0.70, $tan\phi_{res}$=0.40, χ_0=2MPa, c_0=7MPa, G^{I}_{F}=0.03 Nmm, G^{II}_{F}=0.3 Nmm, σ_{dil}=40MPa. For the mortar-mortar interfaces the same parameters are used with the exception of χ_0=4MPa, c_0=14MPa and G^{I}_{F}=0.06 Nmm (and therefore, G^{II}_{F}=0.6 Nmm).

4.1 2D mesh

A mesh of 6 cm side with 4 aggregates per side is used (1720 nodes, 1272 continuous medium elements and 650 zero-thickness inteface elements). It is simulated that the mesh is immersed in a solution of sodium sulfate on the four outer edges (Dirichlet condition). The mechanical calculation is carried out under conditions of plane stress. Figure 3 shows the evolution of sulfate penetration for four different ages, Figure 4 shows the concentrations of precipitated ettringite for those same times and in Figure 5 presents the deformed configuration corresponding to 540 and 740 days.

Figure 3 shows the progressive ingress of sulfates from the edges to the center of the sample. For the last time shown (740 days) sulfates have advanced considerably with values similar to the external concentration in most areas except in the central zone (Fig. 3d).

Figure 4 shows that the ettringite formation front advances towards the center of the sample as time passes. Ettringite precipitation is delayed with respect to the advance of the sulfates, due the reaction rate. Figure 5, shows the deformation of the mesh at 540 and 740 days. In that figure, one can see a perimeter cracking that practically has formed a closed line (spalling) for the last graphical age (740 days).

4.2 3D mesh

In this case, a 4cm side 3D cubic mesh with 28 aggregates is used (35673 nodes, 12749 continuum elements and 18346 zero-thickness interface elements). The specimen (Figure 6) represents a quarter of a pillar, with boundary conditions for the mechanical problem that restrict the movement in the normal direction of all faces in contact with the rest of the pillar material (see Figure 9). For the diffusion problem, unlike the 2D case, a convective boundary condition is applied to these free faces. The reason for applying this condition is that, unlike the 2D mesh and due to its complexity, the 3D mesh has not been refined in the area close to the surfaces in contact with the sulfates, and when applying plain Dirichlet conditions it results in numerical oscillations and negative values of sulfate concentrations, both in the matrix and in the aggregates. In contrast to the 2D case, in 3D there are faces of aggregates that are on the edges of the specimen, and for this reason the code has been modified and the aggregates do not intervene in the diffusion-reaction analysis.

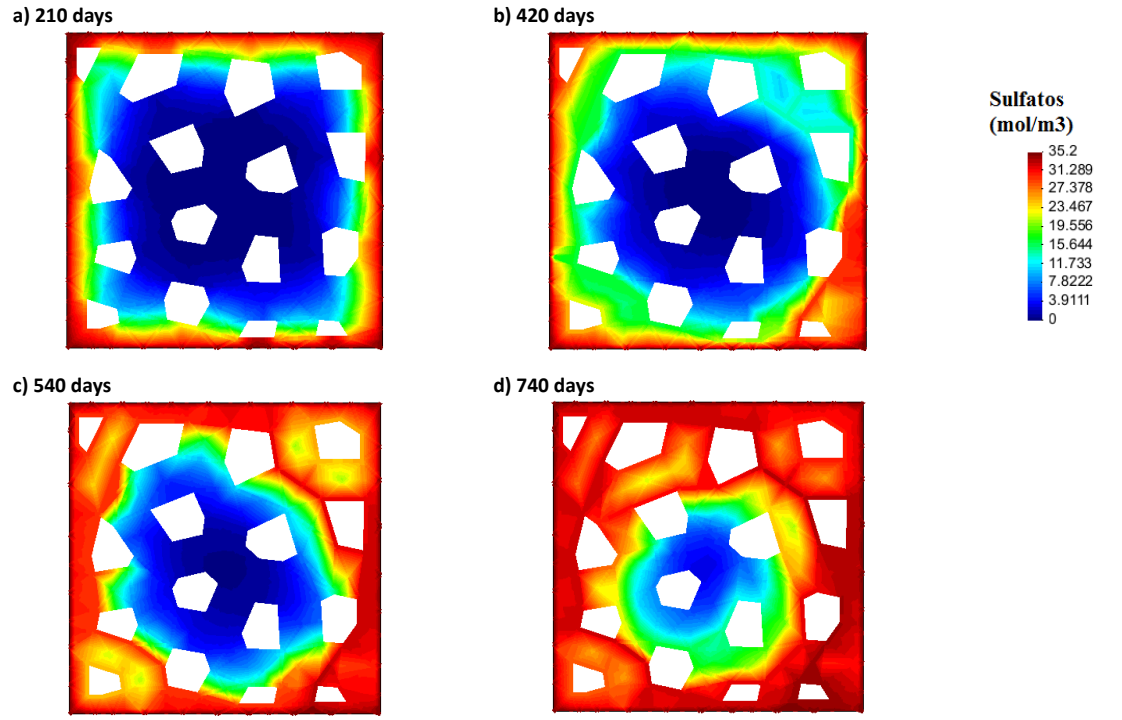

Figure 3: Sulfate progress for the following time values: a) 210 days, b) 420 days, c) 540 days and d) 740 days.

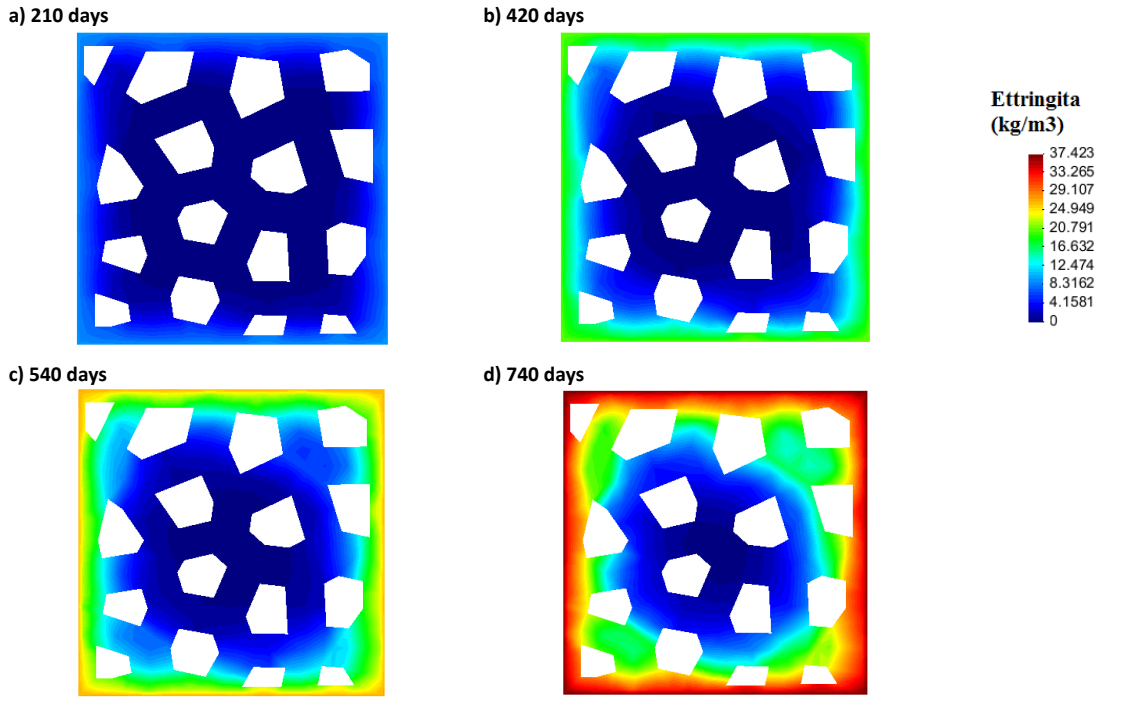

Figure 4: Ettringite precipitation due to the intrusion of the sulfates for the following time values: a) 210 days, b) 420 days, c) 540days and d) 740 days.

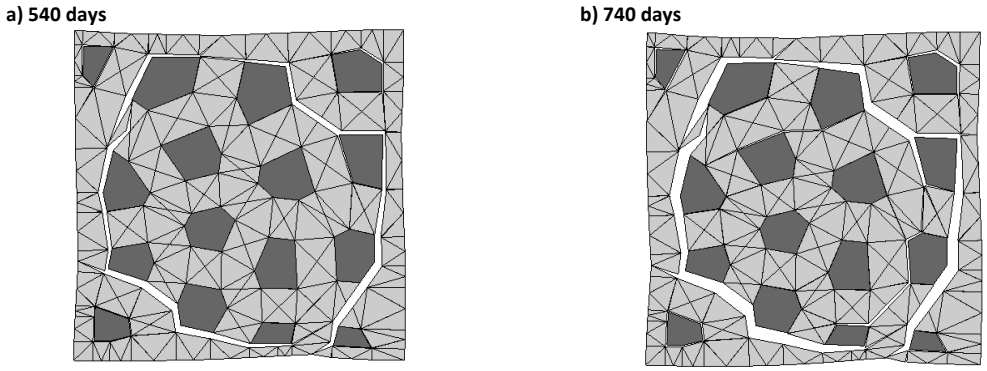

Figure 5: Deformed mesh for the following time values: a) 540 days and b) 740 days (deformation factor x50).

Figure 7 shows the distribution of sulfates and Figure 8 shows the precipitation of ettringite for the ages of 250, 450 and 740 days, from two different perspectives and without representing the aggregates, which allows to appreciate the corresponding penetration towards the interior of the mortar matrix.

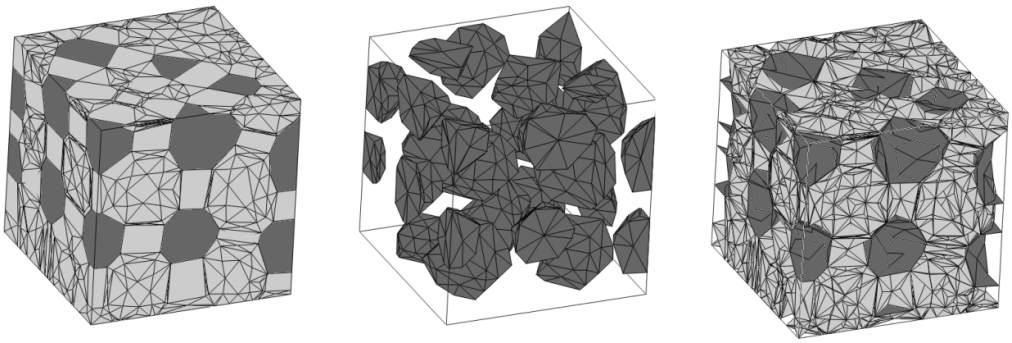

Figure 6: 3D mesh: representation of the mortar and aggregate phases (left), only the aggregates (center) and the two families of interfaces (right): aggregate-mortar (dark gray) and mortar-mortar (gray) interfaces.

As expected, the sulfate penetration front (Fig. 7) and the formation of ettringite (Fig. 8) in the mortar matrix from the two lateral edges towards the center of the sample are observed. However, Figure 7 shows that the sulfate advance occurs in a more attenuated and uniform manner if compared to the 2D results shown in Figure 3. These 3D results seem to be closed to the 2D uncoupled behavior, as shown in Figure 9, where the sulfate advance of the 3D case (right) is compared with the 2D case decoupled (left) at the age of 740 days.

Figure 10 shows the results of the deformation and the work consumed during the cracking process at 740 days. The column on the left shows the results as seen from a top view, and the right column shows them in side-view. Figure 10a clearly shows that at the corner of the faces in contact with the sulfate there is a concentration of volumetric deformations, which results in the formation of fractures. In Figures 10c and 10e it is observed that these fractures are located in vertical planes inclined with respect to the corner. The graphs on the right show that the main planes of fracture propagate vertically along the sample, running in between two rows of aggregates. It is observed that the cracks reach the edges in contact to the sulfates, and

therefore should become preferential paths of penetration and accelerate the deterioration process. However, this effect appears in the 2D analysis but does not occur in the 3D case.

Probably, the anomalous behavior is due to the fact that the convective-type boundary condition generates lower sulfate concentration values at the interface nodes located on the boundaries, resulting in much lower localized inflow *via* open cracks than in the 2D analysis.

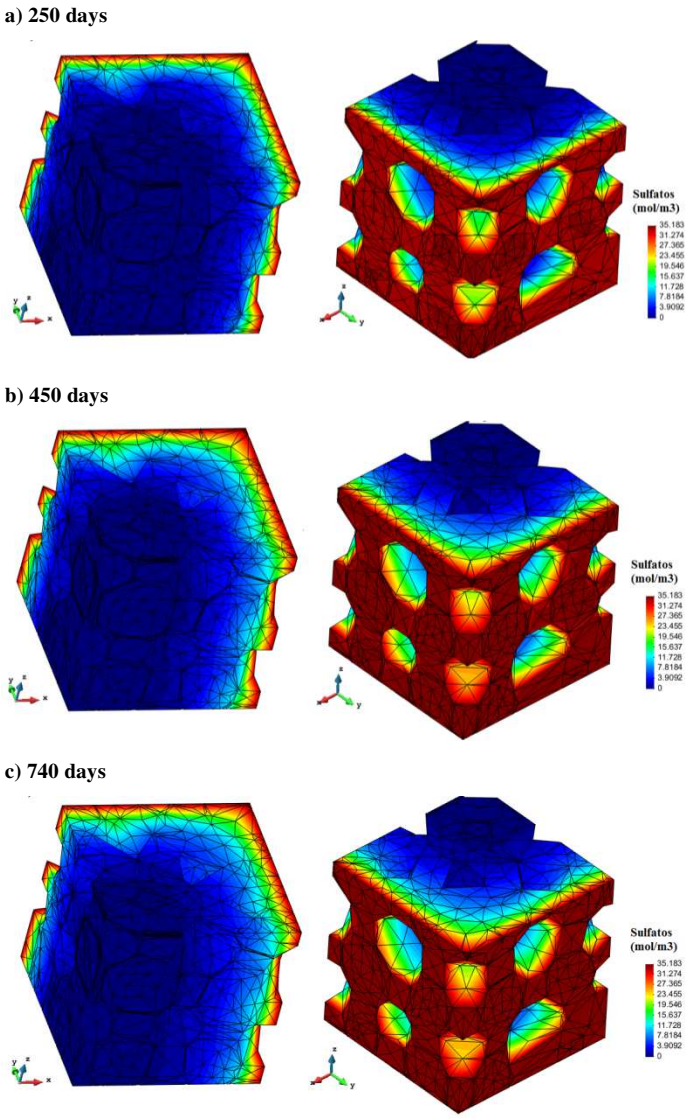

Figure 7: 3D representation of sulfate concentrations for: a) 250 days, b) 450 days and c) 740 days.

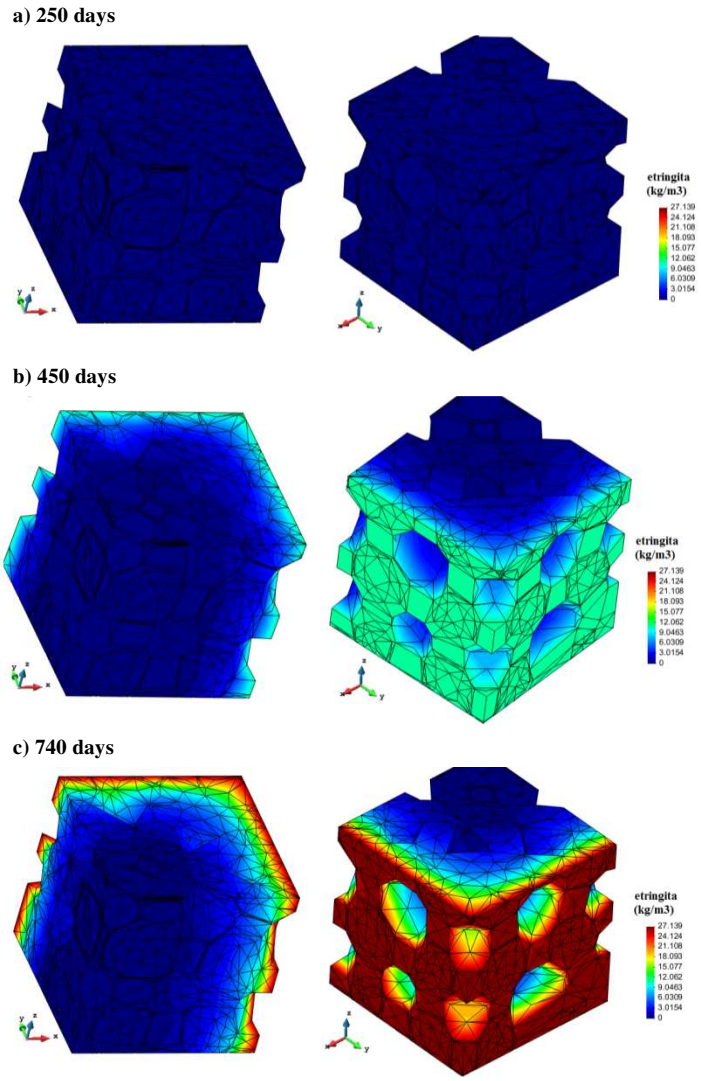

Figure 8: 3D representation of ettringite precipitation for the following time values: a) 250 days, b) 450 days and c) 740 days.

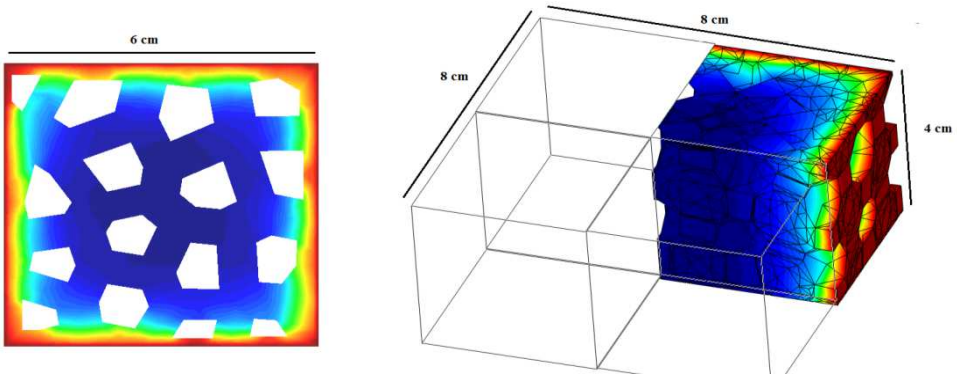

Figure 9: Representation of the sulfate advance front: 2D decoupled (left) and 3D coupled (right) at the age of 740 days.

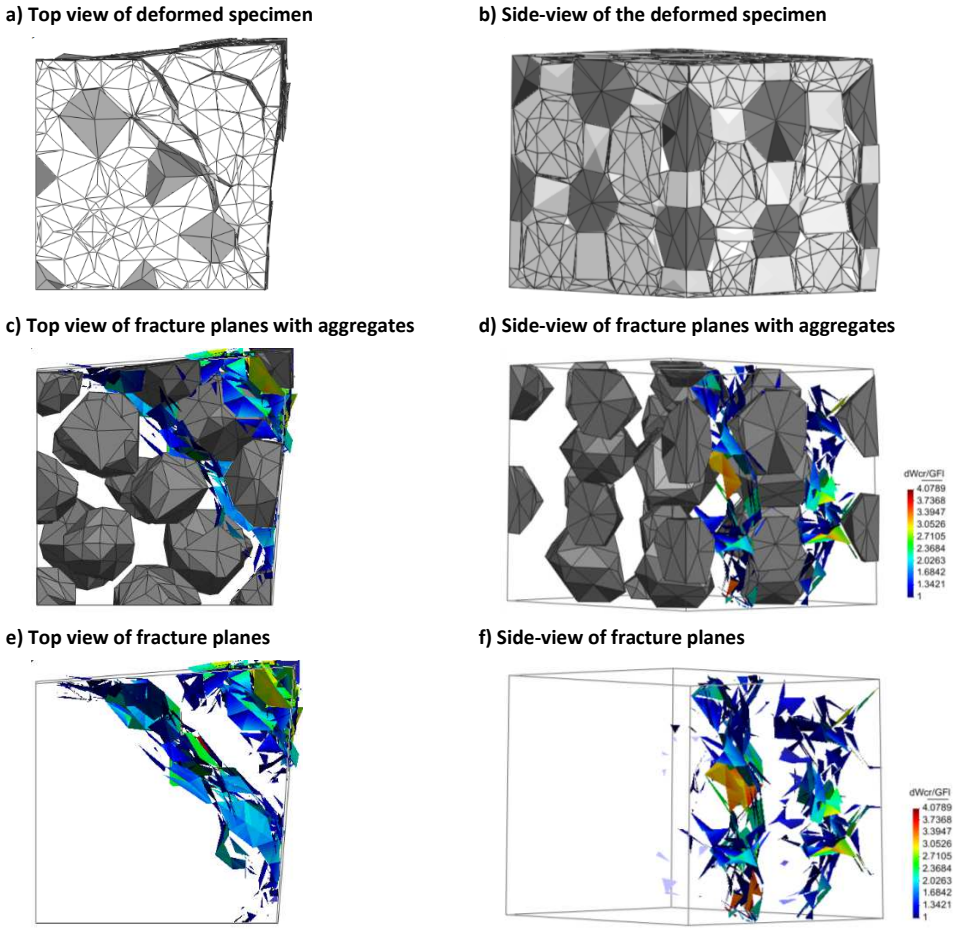

Figure 10: 3D deformed mesh (factor x50) and work dissipated by the fracture process at the age of 740 days.

5 CONCLUDING REMARKS

The 2D coupled results show that the model is able to simulate that, as the interfaces open, creating new channels, the sulfate ingress increases drastically thus forming penetration fronts into the sample. A preliminary 3D coupled analysis has shown that, in terms of depth and penetration of the sulfates and cracking scheme, the results obtained are more similar to those obtained from the 2D uncoupled analysis than to the coupled 2D analysis. In a first interpretation this fact could be explained on the basis of the boundary conditions imposed (of the Newmann-convective type) which were used in order to overcome a lack of mesh refinement near the specimen surface. Current work is oriented to verify this conjecture, and to run the analysis of a more refined 3D cube specimen so that Dirichlet boundary conditions can be applied directly on the specimen surface.

ACKNOWLEDGMENTS

This research is supported by grants BIA2016-76543-R funded by MEC (Madrid), which includes FEDER funds, 2014SGR-1523 from AGAUR-Generalitat de Catalunya (Barcelona) and under a FPU doctoral fellowship (FPU13/02185) from MEC (Madrid) to the first author.

REFERENCES

[1] Collepardi, M. A state-of-the-art review on delayed ettringite attack on concrete. *Cem. Concr. Comp.*, **25**:401-407 (2003).

[2] Lee, S., Hooton, R., Jung, H., Park, D., Choi, C., Effect of limestone filler on the deterioration of mortars and pastes exposed to sulfate solutions at ambient temperature. *Cem. Concr. Res.*, **38**:68-76, (2008).

[3] Brown, P. and Hooton, H., Ettringite and thaumasite formation in laboratory concretes prepared using sul-fate-resisting cements. *Cem. Concr. Comp.*, **24**:361-70 (2002).

[4] Al-Amoudi, O., Attack on plain and blended cements exposed to aggressive sulfate environments. *Cem. Concr. Comp.*, **24**:305-316 (2002).

[5] Irassar, E., Bonavetti, V. and González, M., Micro-structural study of sulfate attack on ordinary and limestone Portland cements at ambient temperature. *Cem. Concr. Res.*, **33**:31-41 (2003).

[6] Carol, I., Prat, P. C., López, C.M. A normal/shear cracking model. Application to discrete crack analysis. *Engng.Mech. ASCE*, **123**:765–773 (1997).

[7] Carol, I., López, C.M. and Roa, O. Micromechanical analysis of quasi-brittle materials using fracture-based interface elements. *Int. J. Num. Meth. Engng*. **52**:193-215 (2001).

[8] Idiart, A., *Coupled analysis of degradation processes in concrete specimens at the meso-level*. Ph.D. Thesis. UPC, Barcelona, (2009).

[9] Idiart, A., López, C.M. and Carol, I. Chemo-mechanical analysis of concrete cracking and degradation due to external sulfate attack: A meso-scale model, *Cem. Concr. Comp.*, **33**:411-423 (2011).

[10] Riera, C. *Advanced Modeling of fracture problems in concrete due to external sulfate attack*. Graduation Thesis for the degree of Geological Engineering, ETSECCPB (School of Civil Engineering)-UPC, Barcelona (in Spanish) (2015).

[11] Riera, C. *3D mesomechanical modeling of external sulphate attack on concrete*. Master Thesis in Geotechnical Engineering, ETSECCPB (School of Civil Engineering)-UPC, Barcelona (in Spanish) (2016).

[12] Tixier, R., Mobasher, B., Modeling of damage in cement-based materials subjected to external sulfate attack. I: Formulation. *J. of Mat. In Civil Engng, ASCE*, **15(4)**:305-313 (2003).

[13] Caballero, A., Carol, I., López C. M. 3D mesomechanical analysis of concrete specimens under biaxial loading. *Fatigue and Fracture Engng. Materials and Structures*, **30**:877-886 (2007).

[14] López C.M., Carol I., Aguado A. Meso-structural study of concrete fracture using interface elements. I: numerical model and tensile behavior. *Materials and Structures*, **41(3)**:583-599 (2008).

[15] López C.M., Carol I., Aguado A. Meso-structural study of concrete fracture using interface element II: compression, biaxial and Brazilian test. *Materials and Structures*, **41(3)**:601-620 (2008).

[16] Segura, J.M., Carol, I., Coupled HM analysis using zero-thickness interface elements with double nodes. Part I: Theoretical model and Part II: Verification and application. *Int. J. Numer. Anal. Meth. Geomech*. **32**:2083–2123, (2008).